

# On the growth and form of the gut

Thierry Savin<sup>1†\*</sup>, Natasza A. Kurpios<sup>2†\*</sup>, Amy E. Shyer<sup>2\*</sup>, Patricia Florescu<sup>1</sup>, Haiyi Liang<sup>1‡</sup>, L. Mahadevan<sup>1,3,4,5,6,7</sup> & Clifford J. Tabin<sup>2</sup>

**The developing vertebrate gut tube forms a reproducible looped pattern as it grows into the body cavity. Here we use developmental experiments to eliminate alternative models and show that gut looping morphogenesis is driven by the homogeneous and isotropic forces that arise from the relative growth between the gut tube and the anchoring dorsal mesenteric sheet, tissues that grow at different rates. A simple physical mimic, using a differentially strained composite of a pliable rubber tube and a soft latex sheet is consistent with this mechanism and produces similar patterns. We devise a mathematical theory and a computational model for the number, size and shape of intestinal loops based solely on the measurable geometry, elasticity and relative growth of the tissues. The predictions of our theory are quantitatively consistent with observations of intestinal loops at different stages of development in the chick embryo. Our model also accounts for the qualitative and quantitative variation in the distinct gut looping patterns seen in a variety of species including quail, finch and mouse, illuminating how the simple macroscopic mechanics of differential growth drives the morphology of the developing gut.**

Understanding morphogenesis, the origin of shape in anatomical structures, organs and organisms, has always been a central goal of developmental biology. Historically, the subject focused on the morphology and dynamics of embryonic growth<sup>1</sup>, with many analogies to observable physical phenomena. This metaphoric approach to biological shape is epitomized in D'Arcy Thompson's *On Growth and Form*<sup>2</sup>, with its focus on a mathematical and physical approach to the subject, emphasizing the role of differential growth in determining form. However, with the modern revolution in molecular biology, the field focused on a framework built around gene regulation, signalling molecules and transcription factors. This led to much insight into the logic of the developmental networks controlling processes as diverse as the patterning of the limb skeleton<sup>3</sup> and the branching morphogenesis of the lung<sup>4</sup>. More recently, however, there has been a renewed appreciation of the fact that to understand morphogenesis in three dimensions, it is necessary to combine molecular insights (genes and morphogens) with knowledge of physical processes (transport, deformation and flow) generated by growing tissues.

In this context, there has been only recent limited exploration of the role of tissue-scale mechanical forces in organogenesis<sup>5–10</sup>. Such large-scale forces can become important when the shape of an organ is remodelled after its initial structure has been formed. An important example of this hierarchy is the looping morphogenesis of the gut<sup>11</sup>. The midgut forms as a simple linear tube of circular cross-section running down the midline of the embryo, and grows at a greater rate than the surrounding tissue, eventually becoming significantly longer than the trunk. As the size of the developing mid- and hindgut exceeds the capacity of the embryonic body cavity, a primary loop is forced ventrally into the umbilicus (in mammals) or yolk stalk (in birds). This loop first rotates anticlockwise by 90° and then by another 180° during the subsequent retraction into the body cavity. Eventually, the rostral half of the loop forms the midgut (small intestine) and the caudal half forms the upper half of the hindgut (the ascending colon).

The chirality of this gut rotation is directed by left–right asymmetries in cellular architecture that arise within the dorsal mesentery<sup>12–14</sup>, an initially thick and short structure along the dorsal–ventral axis through which the gut tube is attached to the abdominal wall. This leads the mesentery to tilt the gut tube leftwards with a resulting anticlockwise corkscrewing of the gut as it herniates<sup>12,13</sup>. However, the gut rotation is insufficient to pack the entire small intestine into the body cavity, and additional loops are formed as the intestine bends and twists even as it elongates. Once the gut attains its final form, which is highly stereotypical in a given species, the loops retract into the body cavity. During further growth of the juvenile, no additional loops are formed<sup>15</sup>, as they are tacked down by fascia, which restrict movement and additional morphogenesis without inhibiting globally uniform growth.

## Relative growth between gut and attached mesentery drives looping

Throughout development, the gut tube remains attached to the body wall along its entire length by the dorsal mesentery, and is fixed at both its rostral and its caudal ends to the mouth and anus, respectively, resulting in the preservation of its connectivity and chirality during growth. The resulting number, shape and size of loops are also conserved in any given species, as shown in Fig. 1a for the chick at embryonic day 16 (E16).

In principle, this regularity of looping could result from either the intrinsic properties of the gut tube and mesentery or from external spatial packing constraints. However, surgical dissection of the gut and mesentery from the rest of the embryonic tissues shows that all the loops remain intact and identical to their *in ovo* structure at various stages of development (Fig. 1a), ruling out any role for body-cavity-induced constraints. Another possible mechanism for the reproducible looping is an increased asymmetric proliferation of cells in the gut tube at the locations of the bends. To test this, we counted the numbers of mitotic cells in the entire midgut section

<sup>1</sup>School of Engineering and Applied Sciences, Harvard University, Cambridge, Massachusetts 02138, USA. <sup>2</sup>Department of Genetics, Harvard Medical School, Boston, Massachusetts 02115, USA.

<sup>3</sup>Department of Organismic and Evolutionary Biology, Harvard University, Cambridge, Massachusetts 02138, USA. <sup>4</sup>Department of Physics, Harvard University, Cambridge, Massachusetts 02138, USA.

<sup>5</sup>Department of Systems Biology, Harvard Medical School, Boston, Massachusetts 02115, USA. <sup>6</sup>Wyss Institute for Biologically Inspired Engineering, Harvard University, Cambridge, Massachusetts 02138, USA.

<sup>7</sup>Kavli Institute for Bionano Science and Technology, Harvard University, Cambridge, Massachusetts 02138, USA. †Present addresses: Department of Materials, Polymer Physics, ETH Zürich, 8093 Zürich, Switzerland (T.S.); Department of Molecular Medicine, Cornell University, Ithaca, New York 14853, USA (N.A.K.); Department of Modern Mechanics, USTC-Hefei, Anhui 230027, China (H.L.).

\*These authors contributed equally to this work.

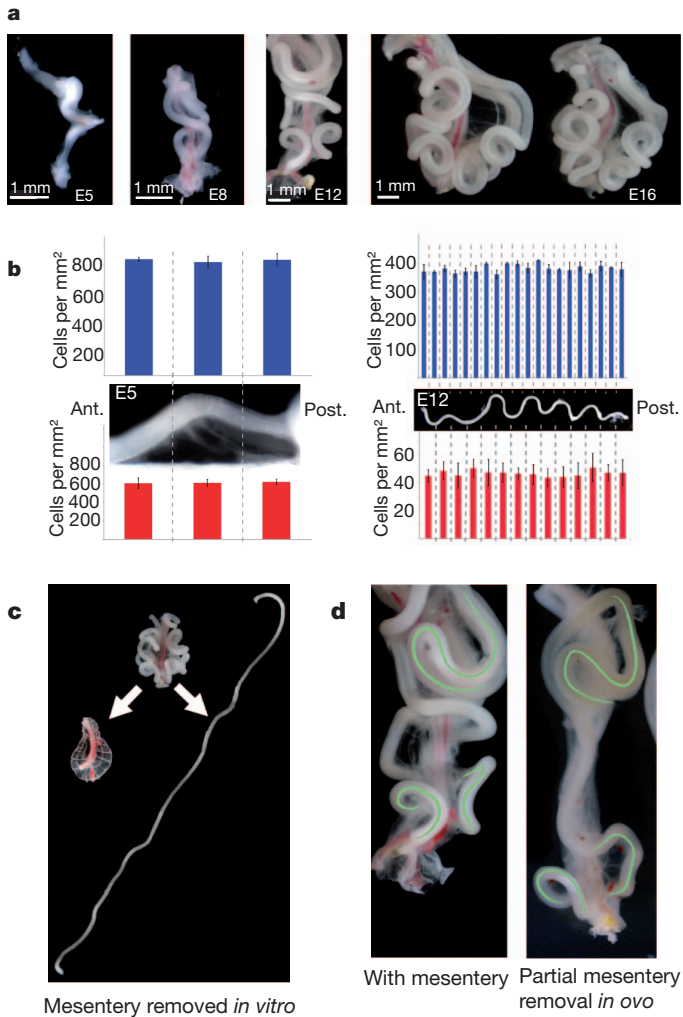


**Figure 1 | Morphology of loops in the chick gut.** **a**, Chick gut at embryonic day 5 (E5), E8, E12 and E16 shows stereotypical looping pattern. **b**, Proliferation in the E5 (left) and E12 (right) gut tubes (blue) and mesentery (red). Each blue bar represents the average number of phospho-H3-positive cells per unit surface in 40 (E5) or 50 (E12) 10- $\mu$ m sections. Each red bar represents the average number of phospho-H3-positive cells per unit surface over six 10- $\mu$ m sections (E5) or in specific regions demarcated by vasculature along the mesentery (E12). The inset images of the chick guts align the proliferation data with the locations of loops (all measurements were made in three or more chick samples). Ant., anterior; post., posterior. Error bars, s.d. **c**, The gut and mesentery before and after surgical separation at E14 show that the mesentery shrinks while the gut tube straightens out almost completely. **d**, The E12 chick gut under normal development with the mesentery (left) and after *in ovo* surgical separation of the mesentery at E4 (right). The gut and mesentery repair their attachment, leading to some regions of normal looping (green). However, a portion of the gut lacks normal loops as a result of disrupting the gut–mesentery interaction over the time these loops would otherwise have developed.

during the formation of the first loop at E5 (Fig. 1b) and later when there were nine loops (E12) (Fig. 1b). We observed consistently uniform proliferation with no significant differences along the rostrocaudal axis of the gut tube, including at loop formation locations and between loops, as well as no observable azimuthal or radial differences in proliferation rates at different cross-sections (Supplementary Fig. 1), consistent with observations that the embryonic gut tube cross-section remains circular along its length.

Because spatial constraints from the body cavity and the gut tube alone cannot explain the reproducible looping, we instead considered the dorsal mesentery, the webbed tissue that attaches the gut tube to

the embryo along its length. As looping morphogenesis is initiated, the dorsal mesentery changes from a thick, asymmetric, multilayer structure to a thin, double-epithelial sheet with no observable left–right asymmetry (Supplementary Fig. 2).

To test whether the dorsal mesentery is integral to the intestinal loops, we separated it from the gut surgically or enzymatically and found that the intestine uncoils into a straight tube, indicating that it was under compression. Simultaneously, the unconstrained dorsal mesentery contracts when freed from the gut tube (Fig. 1c), indicating that this tissue is under tension. Thus the gut–mesentery composite is required to maintain the mature loops in the gut.

To find out whether the dorsal mesentery is also required for the formation of the loops, we surgically separated a portion of the dorsal mesentery from the gut *in ovo*, beginning immediately caudal to the cranial (superior) mesenteric artery (SMA), at day E4, before loops develop. Strikingly, where the mesentery and gut were separated, the intestinal loops failed to form (Fig. 1d) even as normal loops formed in locations rostral and caudal to it (Fig. 1d, green lines). Although we were unable to cut the dorsal SMA *in ovo* during gut loop development, once the loops had matured (E12), surgical dissection of the SMA left the loops intact and in fact highlighted their periodic structure (Fig. 2c). This rules out any possible requirement for the SMA in directing loop structure, and for the vasculature as well, as secondary vessels develop only after the loops themselves have formed.

Although the gut grows uniformly, to investigate whether the mesentery might grow inhomogeneously and thus force the gut to loop at precise locations, we examined the proliferation rate of the mesentery at E5 and at E12. There were no observed differences along the rostrocaudal axis (Fig. 1b), suggesting that the growing mesentery exerts uniform compression along the length of the gut, countered by an equal and opposite tensile reaction on the mesentery from the gut.

Taken together, our observations suggest that uniform differential growth between the gut and the mesentery could be at the origin of loop formation. Because the gut tube is slender, with a length that is much larger than its radius, it responds physically to the differential strain-induced compression from the attached mesentery by bending and looping, while remaining attached to the embryo rostrocaudally. Most importantly, the fact that the gut relaxes to a straight configuration whereas the mesentery relaxes to an almost flat configuration implies that the tissues behave elastically, a fact that will allow us to quantify the process simply.

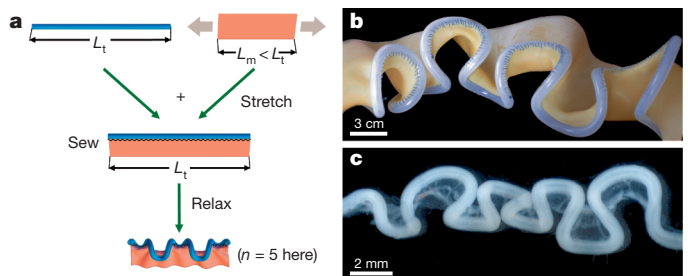


**Figure 2 | Rubber simulacrum of gut looping morphogenesis.** **a**, To construct the rubber model of looping, a thin rubber sheet (mesentery) was stretched uniformly along its length and then stitched to a straight, unstretched rubber tube (gut) along its boundary; the differential strain mimics the differential growth of the two tissues. The system was then allowed to relax, free of any external forces. **b**, On relaxation, the composite rubber model deformed into a structure very similar to the chick gut (here the thickness of the sheet is 1.3 mm and its Young's modulus is 1.3 MPa, and the radius of the tube is 4.8 mm, its thickness is 2.4 mm and its Young's modulus is 1.1 MPa; see Supplementary Information for details). **c**, Chick gut at E12. The superior mesenteric artery has been cut out (but not the mesentery), allowing the gut to be displayed aligned without altering its loop pattern.

### Physical model of gut looping

To investigate the physical origins of this looping pattern, we developed a simple simulacrum of the gut–mesentery composite using a silicone rubber tube (mimicking the gut) and a thin latex sheet (mimicking the mesentery; see Supplementary Information). The differential strain induced by relative growth between the gut and the mesentery is simulated by extending the latex sheet along its length and stitching it to the wall of the naturally straight, unstretched rubber tube along the edge parallel to the direction of membrane stretching (Fig. 2a). On removing all external loads from the composite system, we observe the spontaneous formation of loops in the tube very similar in shape to the looping patterns seen *in ovo* (Fig. 2b). Varying the differential strain, the thickness of the latex sheet, the radius of the rubber tube and their material properties (Supplementary Information) shows that the wavelength and amplitude of the repeating loops depend only on these measurable parameters.

### Scaling laws for loop period, radius and number

We now quantify the simple physical picture for looping sketched above to derive expressions for the size of a loop, characterized by the contour length,  $\lambda$ , and mean radius of curvature,  $R$ , of a single period (Fig. 3a). The geometry of the growing gut is characterized by the gut’s inner and outer radii,  $r_i$  and  $r_o$ , which are much smaller than its increasing length, whereas that of the mesentery is described by its homogeneous thickness,  $h$ , which is much smaller than its other two dimensions. Because the gut tube and mesentery relax to nearly straight, flat states once they are surgically separated, we can model the gut as a one-dimensional elastic filament growing relative to a thin two-dimensional elastic sheet (the mesentery). As the gut length becomes longer than the perimeter of the mesentery to which it is attached, there is a differential strain,  $\varepsilon$ , that compresses the tube axially while extending the periphery of the sheet. When the growth strain is

larger than a critical value,  $\varepsilon_*$ , the straight tube buckles, taking on a wavy shape of characteristic amplitude  $A$  and period  $\lambda \gg A$ . At the onset of buckling, the extensional strain energy of the sheet per wavelength of the pattern is  $U_m \propto E_m \varepsilon_*^2 h \lambda^2$ , where  $E_m$  is the Young’s modulus of the mesentery sheet. The bending energy of the tube per wavelength is  $U_t \propto E_t I_t \kappa^2 \lambda$ , where  $\kappa \propto A/\lambda^2$  is the tube curvature,  $I_t \propto r_o^4 - r_i^4$  is the moment of inertia of the tube and  $E_t$  is the Young’s modulus of the tube. Using the condition that the in-plane strain in the sheet is  $\varepsilon_* \propto A/\lambda$  and minimizing the sum of the two energies with respect to  $\lambda$  then yields a scaling law for the wavelength of the loop:

$$\lambda \propto \left( \frac{E_t I_t}{E_m h} \right)^{1/3} \tag{1}$$

The above theory is valid only at the onset of looping and cannot predict the amplitude or radius of a loop. Far from the onset of the instability, at a strain  $\varepsilon = \varepsilon_0 \gg \varepsilon_*$ , we use a torque balance argument to determine the finite radius of the loop. To deform the gut into a loop of radius  $R$ , the elastic torque required is  $T_t \propto E_t I_t / R$  and must balance the torque exerted by the membrane with strain  $\varepsilon_0$  over a width  $w$  and a length  $R$ , that is,  $T_m \propto E_m h w \varepsilon_0 R$ . The width of this strip is the radial distance from the tube over which the peripheral membrane stretching strain is relaxed, and is determined by the relation  $\varepsilon_0 \propto w/(R - w)$ . Balancing the torques, by equating  $T_t$  with  $T_m$ , and assuming that  $\varepsilon_0 < 1$ , yields the scaling law

$$R \propto \left( \frac{E_t I_t}{E_m h \varepsilon_0^2} \right)^{1/3} \tag{2}$$

### Quantitative geometry and biomechanics of chick gut looping

A comparison of the results of our predictions with quantitative experiments requires the measurement of the geometry of the tissues,

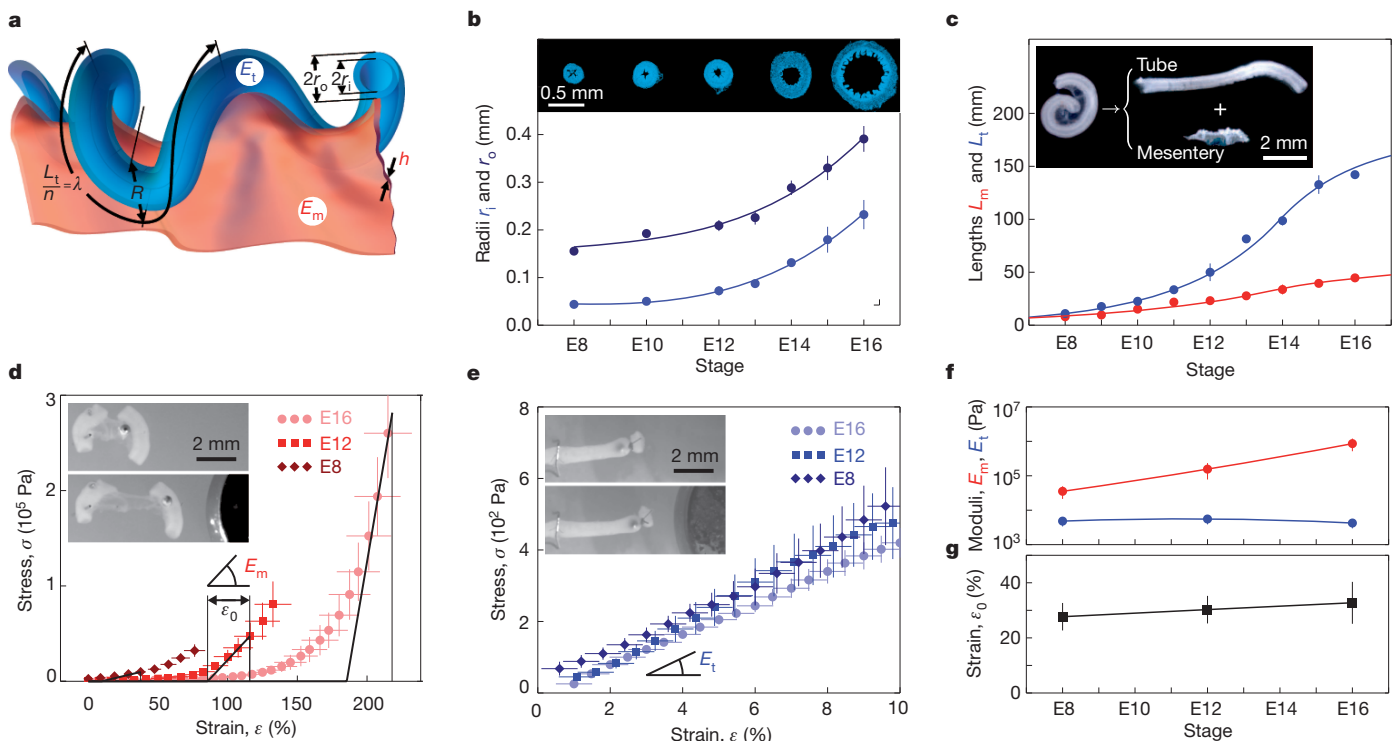


**Figure 3 | Geometric and mechanical measurements of chick gut.**

**a**, Parameters involved in the physical model. **b**, Inner ( $r_i$ , light blue) and outer ( $r_o$ , dark blue) tube diameters. Measurements are extracted from DAPI-stained tube cross-section shown in inset. **c**, Tube (length  $L_t$ , blue) and mesentery (length  $L_m$ , red) differential growth. Inset, length measurement of one isolated loop. **d**, Stress versus strain for the mesentery at E8, E12 and E16. For

physiological strains, we use the linearization shown by the black lines, to extract the effective Young’s modulus,  $E_m$ , and the effective strain,  $\varepsilon_0$ . **e**, Stress versus strain for the gut tube at E8, E12 and E16. **f**, Mesentery and tube Young’s moduli,  $E_m$  (red) and  $E_t$  (blue), at E8, E12 and E16. **g**, Effective differential growth strain,  $\varepsilon_0$ , at E8, E12 and E16. Error bars, s.d.

their elastic properties and the relative strain mismatch at different stages of chick gut development; we chose three stages: E8, E12 and E16 (Fig. 3). The mesentery has a time-varying thickness,  $h$ , which is evaluated from histological cross-section (Supplementary Fig. 2). The inner and outer radii of the gut tube were extracted from 4',6-diamidino-2-phenylindole (DAPI)-stained tube cross-sections (Fig. 3b). The length of the gut tube,  $L_t$ , was measured on the dissected gut. The natural rest length of the periphery of mesentery,  $L_m$ , was measured by cutting out thin strips along the junction with the gut and aligning them unstretched with a ruler (Fig. 3c). The bending stiffness of the gut tube and the stretching stiffness of the mesentery were measured using *in vitro*, uniaxial, low-rate tensile tests, where the load was generated by a magnet applying a calibrated force on a millimetre-size steel ball, attached to one end of a tissue sample that was pinned at the other end. The extension of the sample under load was tracked using videomicroscopy to extract its stress ( $\sigma$ )/strain ( $\varepsilon$ ) response curve (see Fig. 3d, e, insets, Methods and Supplementary Information).

For the mesentery, we observed a nonlinear response curve with a sharp break at a strain  $\varepsilon \leq \varepsilon_p$ , where  $\varepsilon_p = L_t/L_m - 1$  is the physiological strain mismatch, typical of the strain-stiffening seen in biological soft tissues<sup>16</sup>. We define an effective modulus,  $E_m = (d\sigma/d\varepsilon)_{\varepsilon=\varepsilon_p}$ , and strain,  $\varepsilon_0 = (\sigma^{-1} d\sigma/d\varepsilon)_{\varepsilon=\varepsilon_p}^{-1}$ , by locally linearizing the response (Fig. 3d) and noting that the membrane has negligible stiffness when  $0 < \varepsilon < \varepsilon_p - \varepsilon_0$ . For the gut, we measured the modulus,  $E_t = \sigma/\varepsilon$ , from the linear, low-strain response curve ( $\varepsilon < 10\%$ ; Fig. 3e). In Fig. 3f, g, we summarize the variation of  $E_m$ ,  $E_t$  and  $\varepsilon_0$  as functions of developmental time. Measurements of the mesentery stiffness at various locations and in various directions did not show significant differences (Supplementary Fig. 4). This confirms the validity of modelling the mesentery and the gut as isotropic, homogeneous material.

The measured biophysical parameters allowed us to create a detailed numerical simulation of gut looping. Because the gut and mesentery grow slowly, inertial effects are unimportant and the composite system is always in mechanical equilibrium. This equilibrium configuration was calculated as follows. The mesentery was modelled as a discrete elastic membrane consisting of a hexagonal lattice of springs with a discrete energy associated with in-plane stretching/shearing deformations as well as out-of-plane bending deformations<sup>17</sup>, relative to the rest length of the springs. The gut was modelled as an equivalent membrane strip (two elements wide) with a discretized energy associated with bending and stretching deformations, and elastic stiffnesses different from those of the membrane. The geometry, mechanical properties and relative growth of the tissues parameterized by  $h$ ,  $L_t$ ,  $E_m$ ,  $E_t$  and  $\varepsilon_0$  were all experimentally measured at different time points during development. Given these input parameters, energy minimization for different relative growth strains,  $\varepsilon_0$ , yielded predictions for the looping morphology of the gut (Methods and Supplementary Information).

In Fig. 4a, we compare the results of our observation at E16 with numerical simulations. In Fig. 4b, c, we compare our quantitative measurements of the wavelength and radius of curvature of the chick gut at the different measured stages of development (see also Supplementary Fig. 8) with those of both the rubber simulacrum and numerical simulations, as functions of the geometry and elastic moduli of the tube and sheet. Over the strain ranges  $\varepsilon_0 \in [0, 1]$  in the simulation (Supplementary Movie 1) and  $\varepsilon_0 \in [0.5, 1]$  for the various rubber models, we plot the wavelength,  $\lambda$ , and radius,  $R$ , of the loop and find that they follow the relations

$$\lambda \approx 36 \left( \frac{E_t L_t}{E_m h} \right)^{1/3} \quad (3)$$

$$R \approx 4 \left( \frac{E_t L_t}{E_m h \varepsilon_0^2} \right)^{1/3} \quad (4)$$

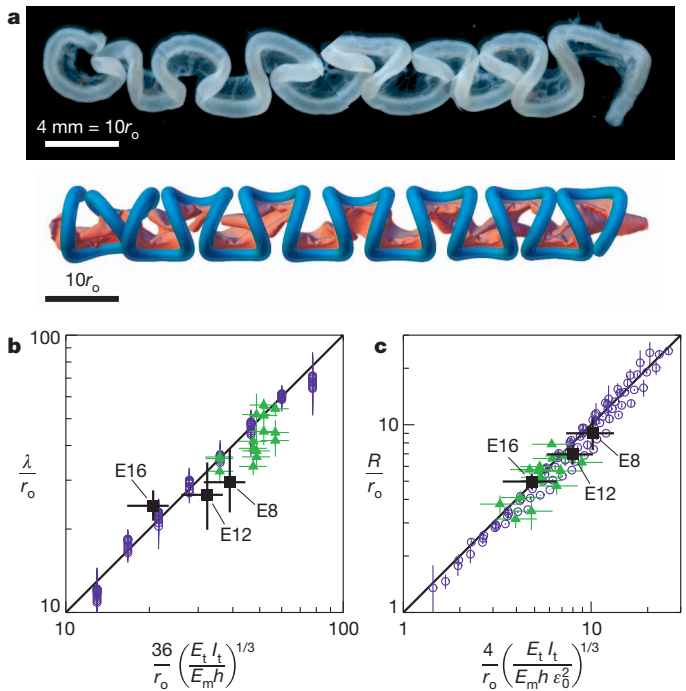


**Figure 4 | Predictions for loop shape, size and number at three stages in chick gut development.** **a**, Comparisons of the chick gut at E16 (top) with its simulated counterpart (bottom). **b**, Scaled loop contour length,  $\lambda/r_0$ , plotted versus the equivalently scaled expression from equation (3) for the chick gut (black squares), the rubber model (green triangles) and numerical simulations (blue circles). The results are consistent with the scaling law in equation (1). **c**, Scaled loop radius,  $R/r_0$ , plotted versus the equivalently scaled expression from equation (4) for the chick gut, the rubber model, and numerical simulations (symbols are as in **b**). The results are consistent with the scaling law in equation (2). Error bars, s.d.

in accord with our simple scaling laws (equations (1) and (2)). In Table 1, we compare the values of these parameters for the chick gut with the expressions given in equations (3) and (4), and confirm that our model captures the salient properties of the looping patterns with no adjustable parameters, strongly suggesting that the main features of the chick gut looping pattern are established by the simple balance of forces induced by the relative growth between the gut and the mesentery.

### Comparative study of gut looping across species

To test our theory in cases other than the development of the chick gut, we took advantage of the distinct gut looping patterns observed in different avian taxa, which have served as criteria for phylogenetic classification and are thought of as having adaptive significance, independent of bird size.

**Table 1 | Morphometry of chick gut looping pattern**

Stage		$n$	$\lambda$ (mm)	$R$ (mm)
E8	Experimental observation	$2.4 \pm 0.4$	$4.6 \pm 1.0$	$1.4 \pm 0.2$
	Computational model*	$1.8 \pm 0.3$	$6.1 \pm 1.5$	$1.6 \pm 0.3$
E12	Experimental observation	$9.0 \pm 0.5$	$5.6 \pm 1.2$	$1.5 \pm 0.1$
	Computational model†	$7.3 \pm 1.6$	$6.8 \pm 1.6$	$1.7 \pm 0.3$
E16	Experimental observation	$15.0 \pm 0.5$	$9.5 \pm 0.5$	$1.9 \pm 0.1$
	Computational model‡	$17.5 \pm 2.4$	$8.1 \pm 1.9$	$1.9 \pm 0.5$

The observed number of loops ( $n$ ), loop wavelength ( $\lambda$ ) and radius ( $R$ ) for the chick at different stages of gut development, for given geometrical and physical parameters associated with the gut and the mesentery, show that the model predictions are quantitatively consistent with observations.

\*  $L_t = 11.0 \pm 0.5$  mm,  $h = 13.0 \pm 1.5$   $\mu$ m,  $r_0 = 155 \pm 8$   $\mu$ m,  $r_t = 44 \pm 5$   $\mu$ m,  $E_m = 35 \pm 14$  kPa,  $E_t = 4.8 \pm 1.4$  kPa,  $\varepsilon_p = 38 \pm 7\%$  and  $\varepsilon_0 = 28 \pm 5\%$ .

†  $L_t = 50.0 \pm 8.3$  mm,  $h = 8.0 \pm 1.5$   $\mu$ m,  $r_0 = 209 \pm 12$   $\mu$ m,  $r_t = 72 \pm 9$   $\mu$ m,  $E_m = 156 \pm 78$  kPa,  $E_t = 5.6 \pm 1.7$  kPa,  $\varepsilon_p = 116 \pm 19\%$  and  $\varepsilon_0 = 30 \pm 5\%$ .

‡  $L_t = 142.1 \pm 3.3$  mm,  $h = 7.1 \pm 1.4$   $\mu$ m,  $r_0 = 391 \pm 27$   $\mu$ m,  $r_t = 232 \pm 31$   $\mu$ m,  $E_m = 861 \pm 344$  kPa,  $E_t = 4.2 \pm 1.3$  kPa,  $\varepsilon_p = 218 \pm 15\%$  and  $\varepsilon_0 = 33 \pm 8\%$ .

We compared the gut looping patterns of the chick with those of the closely related (but differently sized) quail and those of a songbird, the zebra finch. In Fig. 5a, we see that, as previously described<sup>18,19</sup>, the guts of the chick and the quail are organized almost identically but on different scales, and that the digestive tracts of songbirds and chickens are markedly different. To make the comparison quantitative, we repeated the morphometric and mechanical measurements (Supplementary Information) and used them to generate predictions from our scaling theory and computational model. In all cases, the predicted values of  $\lambda$ ,  $R$  and  $n$  are again in excellent agreement with those observed in embryonic guts of the appropriate species (Fig. 5b, c and Table 2). For instance, we find that although growth strains,  $\varepsilon_p$ , are similar between the chick and the quail, the quail mesentery has a tension,  $E_m h \varepsilon_0$ , approximately five times greater than that in the chick mesentery. Qualitatively, this greater elastic force produces a smaller loop, hence inducing more loops per length and, thus, the same number of loops in the smaller bird. By contrast, most of the geometrical and physical parameters characterizing the developing gut and mesentery in the chick and the zebra finch are different and lead to different looping parameters.

Finally, to test our theoretical model with a non-avian example, we performed a similar set of measurements throughout the course of gut development in mouse embryos. In agreement with our findings from birds, the geometrical and biophysical properties of the developing gut and dorsal mesentery suffice to predict accurately the stereotypical patterns of the mature intestinal loops in mouse embryos (Fig. 5 and

**Table 2 | Morphometry of quail, finch and mouse gut looping patterns**

Species and stage		$n$	$\lambda$ (mm)	$R$ (mm)
Quail E12	Experimental observation	$9.0 \pm 0.7$	$4.6 \pm 0.4$	$1.2 \pm 0.1$
	Computational model*	$10.0 \pm 1.3$	$4.1 \pm 1.0$	$1.2 \pm 0.3$
Finch E13	Experimental observation	$5.5 \pm 0.5$	$3.6 \pm 0.5$	$0.6 \pm 0.3$
	Computational model†	$5.3 \pm 0.8$	$3.7 \pm 0.9$	$0.9 \pm 0.2$
Mouse E16.5	Experimental observation	$6.0 \pm 0.5$	$6.0 \pm 0.7$	$0.7 \pm 0.1$
	Computational model‡	$5.6 \pm 0.8$	$6.4 \pm 1.5$	$1.0 \pm 0.1$

The observed number of loops, loop wavelength and radius for the quail, finch and mouse, for given geometrical and physical parameters associated with the gut and the mesentery, show that the model predictions are quantitatively consistent with observations.

\*  $L_t = 41.3 \pm 0.4$  mm,  $h = 14.9 \pm 1.6$   $\mu$ m,  $r_o = 248 \pm 13$   $\mu$ m,  $r_i = 154 \pm 12$   $\mu$ m,  $E_m = 515 \pm 206$  kPa,  $E_t = 4.4 \pm 1.3$  kPa,  $\varepsilon_p = 110 \pm 13\%$  and  $\varepsilon_0 = 23 \pm 5\%$ .  
 †  $L_t = 19.7 \pm 0.8$  mm,  $h = 6.0 \pm 0.6$   $\mu$ m,  $r_o = 227 \pm 14$   $\mu$ m,  $r_i = 120 \pm 13$   $\mu$ m,  $E_m = 802 \pm 321$  kPa,  $E_t = 2.6 \pm 0.8$  kPa,  $\varepsilon_p = 110 \pm 11\%$  and  $\varepsilon_0 = 32 \pm 5\%$ .  
 ‡  $L_t = 35.9 \pm 0.9$  mm,  $h = 12.3 \pm 1.6$   $\mu$ m,  $r_o = 270 \pm 16$   $\mu$ m,  $r_i = 178 \pm 14$   $\mu$ m,  $E_m = 94 \pm 37$  kPa,  $E_t = 1.9 \pm 0.9$  kPa,  $\varepsilon_p = 200 \pm 13\%$  and  $\varepsilon_0 = 64 \pm 5\%$ .

Table 2). The mouse gut is notably characterized by softer tissues and higher mismatch strain, producing tightly coiled loops, as seen in Fig. 5a. The physiological stresses in the mesentery fall in the same range (Supplementary Information) in all the species investigated in this study, suggesting that both growth and the properties of tissues might be regulated by mechanical feedback.

**Discussion**

The developing intestine is a simple, elongated, tubular structure that is stereotypically and reproducibly folded into a compact organ through the process of looping morphogenesis. Using a combination of quantitative experiments, computations and scaling arguments, we have shown that the associated looping patterns are quantitatively determined by the differential growth between the gut tube and the dorsal mesentery and by their geometric and elastic properties, both within individual organisms and across species. We thus bring a quantitative biomechanical perspective to the mostly metaphoric arguments in *On Growth and Form*<sup>2</sup>.

The simplicity of the mechanical origin in the diversity in gut looping patterns, long associated with the adaptive significance of the distinct diets and gut residence times of different animals<sup>18</sup>, also suggests that because it is sufficient to modulate the uniform tissue growth rates, tissue geometry and elasticity of the gut–mesentery system to change these patterns, this is the minimal set of properties on which selection has acted to achieve the looping patterns found in nature.

Identification of the relevant cellular parameters influencing gut morphogenesis opens the door to future studies of the genes involved in controlling cell proliferation and matrix formation in space and time, and sets the stage to understanding the processes by which biochemical and biophysical events across scales conspire to drive the developmental regulation of growing tissues.

**METHODS SUMMARY**

**Embryos.** Fertile chick eggs (White Leghorn eggs) were obtained from commercial sources. Fertile zebra finch eggs were provided by the laboratory of T. Gardner at Boston University. Fertile Japanese quail eggs were obtained from Strickland Game Bird. All eggs were incubated at 37.5 °C and staged following ref. 20. Mouse embryos were collected from staged pregnant females (Charles River Laboratories).

**Immunohistochemistry and histology.** Small intestines were collected from chick embryos at desired stages and fixed in 4% paraformaldehyde in PBS and embedded in paraffin wax. Immunohistochemistry and histology was performed on 10- $\mu$ m transverse sections of the gut tube.

**In ovo gut surgeries.** The gut tube and the dorsal mesentery were separated *in ovo* at stage 23–25 by using a pulled glass needle to cut the connection between the two tissues. Embryos were re-incubated until E12, when they were collected to examine the resulting looping pattern.

**Mechanical properties of gut and mesentery tissue.** The force,  $F(d)$ , between a permanent magnet (The Magnet Source) and millimetre-size steel balls (New England Miniature Ball Corp.), separated by a distance  $d$ , was calculated from the damped motion of the ball rising in glycerol with the magnet lowered from

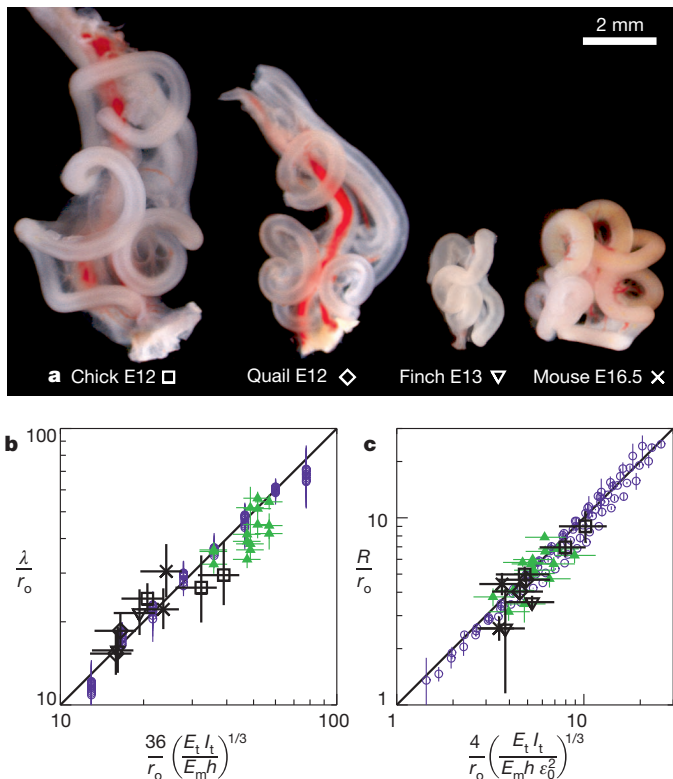


**Figure 5 | Comparative predictions for looping parameters across species.** a, Gut looping patterns in the chick, quail, finch and mouse (to scale) show qualitative similarities in the shape of the loops, although the size and number of loops vary substantially. b, Comparison of the scaled loop contour length,  $\lambda/r_o$ , with the equivalently scaled expression from equation (3) shows that our results are consistent with the scaling law in equation (1) across species. Black symbols are for the animals shown in a, other symbols are the same as in Fig. 4b. c, Comparison of the scaled loop radius,  $R/r_o$ , with the equivalently scaled expression from equation (4) shows that our results are consistent with the scaling law in equation (2) across species (symbols are as in b). In b and c, points are reported for chick at E8, E12 and E16; quail at E12 and E15; finch at E10 and E13; and mouse at E14.5 and E16.5. Error bars, s.d.

above. For  $2\text{ mm} < d < 8\text{ mm}$ , the range used in the subsequent measurements,  $F(d)$  ranges from  $1\text{ }\mu\text{N}$  to  $1\text{ mN}$ . We then surgically extracted strips of the mesentery and sections of the gut tube from fresh animal embryos. A steel bead was attached at one end of the sample, by either gluing it onto the strip or sealing it into the tube. With the other end of the sample pinned to an agarose gel, the magnet was moved closer to stretch the sample while  $d$  and the extension,  $L$ , of the sample were tracked by video. We then calculated the stress,  $\sigma = F(d)/A_0$ , and the strain,  $\epsilon = L/L_0 - 1$ , where  $L_0$  and  $A_0$  are respectively the length and the cross-sectional area of the sample at rest. All dissections, manipulations and tensile tests occurred in Ringer buffer (Sigma Aldrich), and within hours after the surgery.

**Full Methods** and any associated references are available in the online version of the paper at [www.nature.com/nature](http://www.nature.com/nature).

Received 23 January; accepted 7 June 2011.

1. His, W. *Anatomie Menschlicher Embryonen* (Vogel, 1880).
2. Thompson, D. W. *On Growth and Form* (Cambridge Univ. Press, 1917).
3. Johnson, R. L. & Tabin, C. J. Molecular models for vertebrate limb development. *Cell* **90**, 979–990 (1997).
4. Metzger, R. J. & Krasnow, M. A. Genetic control of branching morphogenesis. *Science* **284**, 1635–1639 (1999).
5. Hufnagel, L. *et al.* On the mechanism of wing size determination in fly development. *Proc. Natl Acad. Sci. USA* **104**, 3835–3840 (2007).
6. Beloussov, L. V. *et al.* Mechanical stresses in embryonic tissues: patterns, morphogenetic role, and involvement in regulatory feedback. *Int. Rev. Cytol.* **150**, 1–34 (1994).
7. Taber, L. A. Biomechanics of cardiovascular development. *Annu. Rev. Biomed. Eng.* **3**, 1–25 (2001).
8. Salazar-Ciudad, I. & Jernvall, J. A computational model of teeth and the developmental origins of morphological variation. *Nature* **464**, 583–586 (2010).
9. Hamant, O. *et al.* Developmental patterning by mechanical signals in *Arabidopsis*. *Science* **322**, 1650–1655 (2008).
10. Forgacs, G. & Newman, S. *Biological Physics of the Developing Embryo* (Cambridge Univ. Press, 2005).
11. Schoenwolf, G. *et al.* *Larsen's Human Embryology* Ch. 14 (Elsevier Health Sciences, 2008).
12. Kurpios, N. A. *et al.* The direction of gut looping is established by changes in the extracellular matrix and in cell:cell adhesion. *Proc. Natl Acad. Sci. USA* **105**, 8499–8506 (2008).
13. Davis, N. M. *et al.* The chirality of gut rotation derives from left-right asymmetric changes in the architecture of the dorsal mesentery. *Dev. Cell* **15**, 134–145 (2008).
14. Hecksher-Sorensen, J. *et al.* The splanchnic mesodermal plate directs spleen and pancreatic laterality, and is regulated by *Bapx1/Nkx3.2*. *Development* **131**, 4665–4675 (2004).
15. Kleinman, R. E. *et al.* *Walker's Pediatric Gastrointestinal Disease* 207–216 (Decker, 2008).
16. Fung, Y. C. *Biomechanics: Mechanical Properties of Living Tissues* 2nd edn, 242–320 (Springer, 2004).
17. Liang, H. & Mahadevan, L. The shape of a long leaf. *Proc. Natl Acad. Sci. USA* **106**, 22049–22054 (2009).
18. Beddard, F. E. *The Structure and Classification of Birds* (Longmans, Green and Co., 1898).
19. Mitchell, C. P. On the intestinal tract of birds. *Proc. Zool. Soc. Lond.* **64**, 136–159 (1896).
20. Hamburger, H. & Hamilton, H. L. A series of normal stages in the development of the chick embryo. *J. Exp. Morphol.* **88**, 49–92 (1951).

**Supplementary Information** is linked to the online version of the paper at [www.nature.com/nature](http://www.nature.com/nature).

**Acknowledgements** We thank R. Prum for pointing out to us the literature on avian intestines, and the Harvard NSF MRSEC, the MacArthur Foundation (L.M.) and NIH RO1 HD047360 (C.J.T.) for support.

**Author Contributions** C.J.T., N.A.K. and L.M. designed the research with additional contributions from T.S. and A.E.S.; T.S. (biophysical and computational experiments, data analysis), N.A.K. (biological experiments), A.E.S. (biological and biophysical experiments) and L.M. (physical mechanism, physical/mathematical model, scaling theory) did the research; P.F. (stitched physical model) and H.L. (built computational model) contributed tools; and T.S., N.A.K., L.M. and C.J.T. wrote the paper.

**Author Information** Reprints and permissions information is available at [www.nature.com/reprints](http://www.nature.com/reprints). The authors declare no competing financial interests. Readers are welcome to comment on the online version of this article at [www.nature.com/nature](http://www.nature.com/nature). Correspondence and requests for materials should be addressed to L.M. ([lm@seas.harvard.edu](mailto:lm@seas.harvard.edu)).

## METHODS

**Embryos.** Fertile chick eggs (White Leghorn eggs) were obtained from commercial sources. Fertile zebra finch eggs were provided by the laboratory of T. Gardner at Boston University. Fertile Japanese quail eggs were obtained from Strickland Game Bird. All eggs were incubated at 37.5 °C and staged following ref. 20. Mouse embryos were collected from staged pregnant females (Charles River Laboratories).

**Immunohistochemistry and histology.** Small intestines were collected from chick embryos at desired stages and fixed in 4% paraformaldehyde in PBS and embedded in paraffin wax, allowing for 10- $\mu$ m transverse sections of the gut tube. Fast green staining was performed as described in ref. 20. Immunohistochemistry was performed with rabbit polyclonal antiphospho-H3 (1:100) (Millipore) overnight at 4 °C in PBS containing 3% goat serum and 0.1% Triton X-100. Sections were next incubated with Alexa Fluor 594 goat anti-rabbit secondary antibody (1:300; Molecular Probes) for 1 h at room temperature (25 °C). DAPI (Molecular Probes) was used as a nuclear counterstain and to determine the inner and outer radii of the gut tube.

**In ovo gut surgeries.** The gut tube and the dorsal mesentery were separated *in ovo* at stage 23–25 (ref. 20) by using a pulled glass needle to cut the connection between the two tissues. Most, but not all, of the connection was ablated as care was taken to avoid puncturing the dorsal aorta, which runs over the gut tube and dorsal mesentery at this stage. Embryos were re-incubated until E12, when they were collected to examine the resulting looping pattern.

**Physical simulacrum using rubber.** We used wide strips of elastic rubber sheeting (McMaster-Carr) of various thicknesses. Each strip was held stretched in one direction at the desired extension using clamps, and a silicon rubber tube (NewAge Industries) was stitched to the sheet using sewing thread (Supplementary Information).

**Calibration of the magnetic force.** The attractive interaction between a permanent disc magnet (commercial grade, axially magnetized, neodymium Nd-Fe-B; The Magnet Source) and high-precision steel balls (AISI 440C stainless steel, radii  $r_b = 0.122, 0.253$  and  $0.398$  mm; New England Miniature Ball Corp.) was calibrated using a ‘falling-ball viscometer’ geometry: immersed in a tube filled with pure glycerol, the magnet is brought closer to the ball from above, and the ball consequently rises (we ensured that all materials used to manipulate the beads and the magnet during the measurements, calibration and tensile tests had no magnetic susceptibility). The force exerted by the magnet is balanced by gravity, drag and inertia. At low Reynolds number, drag force and inertia can be measured from the ball trajectory that is extracted using video tracking (see details in the Supplementary Information). We can then calculate the attractive force,  $F(d)$ , between the magnet and the ball as a function of their separation distance,  $d$ . We report our results in Supplementary Fig. 3 and Supplementary Table 1. Notably, for the distances,  $2 \text{ mm} < d < 8 \text{ mm}$ , used in the tissue tensile test, the force ranges from 1  $\mu$ N to 1 mN.

**Measurements of tissue mechanical properties.** We surgically dissected fragments of the mesentery and of the gut tube from live embryos. Samples of the mesentery were cut out to leave a well-defined, millimetre-width strip with principal axis either perpendicular to the tube (radial measurement) or parallel to the tube (tangential measurement). For mesentery fragments, the steel beads were glued using synthetic glue (Instant Krazy Glue) at one end of the tissue strip. The other end was pinned to an agarose gel layer. During the dissection of the sample, we kept sections of the tube or of the superior mesenteric artery to provide convenient handles to which to attach the bead (see Fig. 3d and Supplementary

Fig. 4, where sections of the tube are visible). For gut tube fragments, the steel beads were inserted into the tube and secured by tying the lumen using a hair with an overhand knot. The other end of the tube was held on the agarose gel using a horseshoe pin (Fig. 3e and Supplementary Fig. 5). All dissections, manipulations and tensile tests were performed in Ringer buffer (Sigma Aldrich), and the measurements were made within a few hours of the dissection.

The magnet was attached to a plastic arm held on a micrometric translation stage, and moved closer to the sample on the agarose gel (Supplementary Fig. 4a). The magnet attracted the steel bead and stretched the sample in a controlled fashion (Supplementary Movie 2). The tensile tests were video-recorded to track the extension,  $L$ , of the sample and the bead–magnet distance,  $d$ , and were run as follows. The sample was first pre-conditioned by stretching it once to an extension ratio greater than one, after which the magnet was removed to let the sample relax to its rest length,  $L_0$  (Supplementary Movie 2), at which stage we measured the rest width,  $w_0$ , of the mesentery sample. The magnet was then moved back towards the sample in a stepwise manner. At each step, the sample stretched and was confirmed visually to have reached equilibrium extension before the next step was taken. We thus effectively measured the static elasticity of the tissue, in terms of the nominal stress,  $F(d)/A_0$ , produced by a nominal strain,  $\varepsilon = L/L_0 - 1$ . Here  $A_0$  is the cross-section of the sample at rest:  $A_0 = w_0(1 + \varepsilon_p)^{1/2}h$  for the mesentery, by virtue of material incompressibility, and  $A_0 = \pi(r_o^2 - r_i^2)$  for the tube.

We verified that this method gives reproducible results, and we found that the same-sample variations were less than sample-to-sample variations that we measured at about 50%. Several stress–strain response curves, corresponding to samples of mesentery and gut tubes extracted from different chick E16 embryos are shown in Supplementary Figs 4c and 5b and indicate the level of reproducibility.

**Computational model.** The mesentery was modelled as a hexagonal lattice of linear springs with rest length  $a_m$ , whose discrete energy

$$F_m = \frac{\sqrt{3}E_m h}{4} \sum_{ij} (r_{ij} - a_m)^2 + \frac{E_m h^3}{12\sqrt{3}} \sum_{\alpha\beta} (\mathbf{n}_\alpha - \mathbf{n}_\beta)^2$$

accounts for in-plane stretching (first term, where  $r_{ij}$  is the spring length between nodes  $i$  and  $j$ ) and out-of-plane bending (second term, where  $\mathbf{n}_\alpha$  is the unit normal vector to the triangular facet), and tends to the energy of an elastic membrane of thickness  $h$  and Young’s modulus  $E_m$  as  $a_m \rightarrow 0$  (ref. 17). The gut tube was modelled with a similar, but two-element-wide, lattice of springs with rest length  $a_t$ . The discrete energy

$$F_t = \frac{5.6\sqrt{3}E_t I_t}{8r_o^3} \sum_{ij} (r_{ij} - a_t)^2 + \frac{E_t I_t}{2r_o\sqrt{3}} \sum_{\alpha\beta} (\mathbf{n}_\alpha - \mathbf{n}_\beta)^2$$

of this strip also contains in- and out-of-plane deformations terms (first and second terms, respectively), which are chosen such that the in- and out-of-plane bending stiffnesses both converge to  $E_t I_t$  for a tube of outer radius  $r_o$  (see details in Supplementary Information). At various time points in the development of the gut (E8, E12 and E16), the parameters  $h$ ,  $I_t$ ,  $E_m$ ,  $E_t$  and  $\varepsilon_0$  are all experimentally measured and input into the energy, with the relative growth,  $\varepsilon_0 = a_m/a_t - 1$ , imposing the mismatch strain between the membrane and the tube attached to it. Then the energy  $F_m + F_t$  is minimized using a damped molecular dynamics algorithm<sup>17</sup>, to yield the equilibrium configuration of the gut–mesentery composite system.